Vol. 25, No. 3(2026) Sim26926

Revista Mexicana de Ingeniería Química

Numerical analysis for non-premixed combustion interacting with a free vortex

Análisis numérico de combustión no premezclada interaccionando con un vórtice libre

M.T. Parra[1]*, V. Mendoza[2]

[1] ITAP (Institute for Advanced Production Technologies). Universidad de Valladolid.
[2] Universidad de Valladolid.

Received: July 21, 2026; Accepted: August 30, 2026

Abstract

The present study was carried out with the goal of investigating the effects of swirl intensity on flow fields. For this purpose, a mesh was created to reproduce the benchmark test case developed by Roback and Johnson. With the main objective of properly evaluating the mixing quality inside the combustion chamber, the transport equations were solved to obtain the passive scalar and residence time in the combustion chamber for the isothermal case. The developed flow provides insights into the ways in which the primary flow (axial nozzle) and the secondary flow (annular nozzle) are mixed and the residence time of the flow, targeting the zones where the fluid becomes stagnant (i.e., long residence). The open-source code OpenFOAM® is employed to solve the Reynolds- Averaged Navier–Stokes (RANS) equations with the k-ε standard turbulence model. In the isothermal case, the numerical results demonstrate reasonable agreement with the relevant experimental data, paving the way for an equitable understanding of the recirculation, mixing, and combustion zones. Moreover, a combustion model based on the Eddy Dissipation Concept (EDC) is utilized to identify the zones where reactions are produced and to analyze the variation in the Damköhler number with increasing swirl number.

Keywords: swirling flows; Eddy Dissipation Concept, free vortex, fluid age, non-premixed combustion.

Resumen

El presente estudio se llevó a cabo con el objetivo de investigar los efectos de la intensidad de rotación en los patrones de flujo. Para ello, se creó una malla que reproduce el caso de prueba de referencia desarrollado por Roback y Johnson. Con el objetivo principal de evaluar adecuadamente la calidad de la mezcla dentro de la cámara, se resolvieron las ecuaciones de transporte para obtener las distribuciones del escalar pasivo y del tiempo de residencia en la cámara para el caso isotérmico. El flujo desarrollado proporciona información sobre cómo se mezclan el flujo primario (tobera axial) y el flujo secundario (tobera anular), así como sobre el tiempo de residencia del flujo, centrándose en las zonas donde el fluido se estanca (es decir, residencia prolongada). Se empleó el código de código abierto OpenFOAM® para resolver las ecuaciones de Navier-Stokes promediadas de Reynolds (RANS) con el modelo de turbulencia estándar k-ε. En el caso isotérmico, los resultados numéricos muestran una concordancia razonable con los datos experimentales relevantes, lo que permite una comprensión equitativa de las zonas de recirculación, mezcla. Además, se utiliza un modelo de combustión basado en el concepto de disipación de remolinos (EDC, por sus siglas en inglés) para identificar las zonas donde se producen las reacciones y para analizar la variación del número de Damköhler con el aumento del número de swirl.

Palabras clave: flujos turbulentos; concepto de disipación de torbellinos, vórtices libres, edad del fluido, combustión no premezclada.

*Corresponding author. E-mail: mariateresa.parra@uva.es ;
https://doi.org/10.24275/rmiq/Sim26926
ISSN:1665-2738, *issn-e*: 2395-8472

1 Introduction

In recent years, international regulations for emissions and the increased efficiency of energy conversion devices have motivated governments, industries and academia to develop advanced combustion systems, leading to significant improvements. In this context, there are several challenges to overcome to achieve decarbonization.

Enclosed non-premixed combustion with swirling flows is a configuration frequently used in industrial applications due to its favorable characteristics, including stability of the flame when using lean mixtures, low nitrogen oxide (NOx) emissions and minimal maintenance, increasing the lifetime of the equipment (Syred, 1971 and Zhen, 2011). Flames can be stabilized through a bluff-body orientation (Lai et al, 2026) or the use of swirling blades (Yu *et al.*,2025). With these types of flow, recirculation zones are created inside the chamber, with the interface between these zones characterized by high shear stress, favoring heat transfer between the inlet mixture and the hot gases derived from combustion (Lin, 2025 and Mesquina, 2026). The vortex breakdown mode is one of the most relevant parameters determining the flame shape in swirling flows, thus influencing both the emissions and flame dynamics and characteristics. A previous study (Xu et al, 2026) provided evidence for a tulip-shaped flame stabilized by bubble vortex breakdown and a V-shaped flame stabilized by conical vortex breakdown. Vortex breakdown and the flame shape play key roles in characterizing the emission behaviors of burners; in particular, efficiency can be achieved when the device configuration ensures an appropriate fuel–air mixture and an adequately stable flame, leading to low NOx emissions (Kassem, 2011 and Messig 2013).

Experimental results, together with computational results, constitute fundamental tools in advancing industrial equipment designs (Tlatelpa-Becerro *et al.*, 2026; Martinez-Gutierrez, 2026 and Molina-Herrera, 2026). One of the greatest challenges in numerical computation is capturing the interactions between turbulence and chemical properties (Messig 2013 and Bennett 2000).

Considering the importance of burners with swirling flows as a new technology, several numerical models have been developed to study associated phenomena, including recirculation zones and high velocity gradients, in such burners. These models have been constructed using both commercial and open-source codes (Pfeiler, 2010).

In the present study, the benchmark test case of Roback and Johnson (1983) is reproduced, which involves a simple burner with two coaxial flows: an axial inlet providing an inert gas–fuel mixture and an annular inlet providing a swirling air flow. The expansion of the flow inside the chamber produces an Outer Recirculation Zone (ORZ) at the border and another Inner Recirculation Zone (IRZ) along the central axis. The swirl number and the geometry of the burner directly influence the position and size of the recirculation zones. Experimental velocity profiles in different sections of the chamber are available for the validation of isothermal models.

In this study, a hexahedral mesh was constructed for the domain using the snap-pyHexMesh tool. An idealized swirl generator was designed for the creation of free vortex, and various resolution schemes for the convective term have been designed. In addition, a model for resolution of the passive scalar and age of fluid in the transport equation was implemented in the isothermal case enabling a detailed analysis of the mixing zones to be carried out. Finally, a simplified combustion model named the Eddy Dissipation Concept was applied (Kassem, 2011 and Magnussen 1977).

2 Physical system

In this section, the geometry of the burner used in the test case of Roback and Johnson is described in detail (Roback and Johnson, 1983). The burner basically consists of two coaxial flows—an axial flow where a fuel–gas mixture enters the chamber, and an annular flow where air comes in, with the flow characterized by the swirl number determined according to the vane swirler. Flow expansion at the inlet of the chamber produces a toroidal Outer Recirculation Zone (ORZ). If the swirl number is large enough ($S > 0.6$), the incoming flow causes an inverted flow in the central axis, creating a second Inner Recirculation Zone (IRZ) (Olivani *et al.*, 2007). The location of the flame is directly related to the size and position of the recirculation zones; in particular, the IRZ carries an inverted flow with the hot gases of combustion, thus providing energy for the ignition of the incoming flow with the fresh inert gas–fuel mixture. The mixing of the reactants is improved in the interfacial zone of the two flows, consequently accelerating the combustion process. Figure 1 and Table 1 describe the geometry of the combustion chamber, including the inlets, in detail.

Table 1. Dimensions of the geometric model shown in Figure 1.

R_{i1} [mm]	R_{i2} [mm]	R_a [mm]
12.5	15.3	29.5
R_0 [mm]	L_0 [mm]	L [mm]
61	50	1016

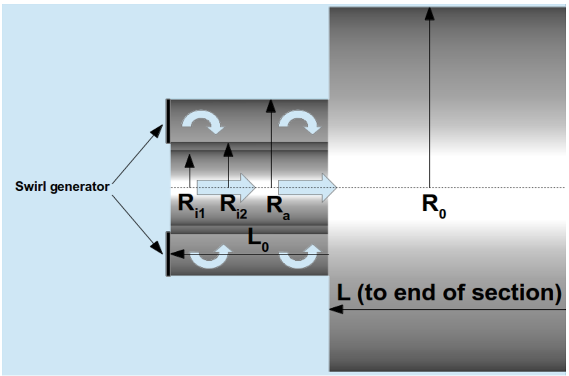

Figure 1. Sketch of the inlets at the entrance of the combustion chamber.

Various parameters have a direct bearing on the characteristics of the fuel injection behavior, including the: geometry of the combustion chamber, fluid velocity, swirl number and fuel–air ratio (Iyogun, 2011 and Cuoci, 2013). This idea constitutes the primary motivation for pursuing the present work.

An idealized swirl generator imposes a velocity distribution that corresponds to a free vortex, which maintains conservation of angular momentum. This ensures that no energy is consumed; no secondary flows appear, due to the equilibrium of pressures in the radial direction; and no forced vortices occur, which move in the manner of a solid with respect to an axis of rotation. The distribution of velocities is configured as a function of the swirl number and the radial distance. As there is no unique definition for the swirl number in the literature, for this particular study, the swirl number is assumed as the ratio between the angular and the axial mean velocities. Vignat (2022) established that the conventional swirl number should be acquired at an axial section as close as possible to the outlet of the injector, as long as Ra/Ri2 > 2.0. References (Lai, 2026 and Li 2025), among others, used the same definition. Equation (1) shows the formal and proposed definitions for swirl number, S, while Equation (2) is the expression that defines a free vortex. The tangential velocity is v_θ at any given radius r whereas the axial velocity is v_z. Figure 2 depicts the imposed velocity field in the annular inlet for a free vortex, where $\bar{r}$ denotes the mean radius of the annular entrance. In this study, the swirl number is assumed to be equal to unity. Recirculation zones are enclosed within the iso-surfaces of zero axial velocity.

$$\mathbf{S} = \frac{\int \rho(\mathbf{r}\mathbf{v}_\theta)\mathbf{v_z} 2\pi \mathbf{rdr}}{\mathbf{R}\int \rho \mathbf{v_z^2} 2\pi \mathbf{rdr}} = \frac{\mathbf{v}_\theta}{\mathbf{v_z}} \tag{1}$$

$$\bar{\mathbf{r}}\cdot\mathbf{v}_\theta = \mathbf{constant} \tag{2}$$

3 Numerical procedure

This section delineates the governing equations for the physical system, the applicable boundary conditions and additional equations for mixing. The whole work was implemented using the open-source CFD tool OpenFOAM®-version 2.3.0 to solve the equations in a 3D domain.

The main characteristics of the flow are three-dimensional, transient, Newtonian, turbulent and incompressible for the Reynolds-Averaged Navier–Stokes (RANS) equations. On the other hand, when there is no reaction, the flow is established as steady.

$$\frac{\partial \rho}{\partial t} + \frac{\partial}{\partial x_i}(\rho \mathrm{u}_i) = 0 \tag{3}$$

$$\frac{\partial \rho \mathrm{u}_i}{\partial t} + \frac{\partial}{\partial x_j}\left(\rho \mathrm{u}_i u_j\right) = -\frac{\partial p}{\partial x_i} + \frac{\partial\left(\tau_{\mathrm{ij}}\right)_{\mathrm{eff}}}{\partial x_j} \tag{4}$$

$$\frac{\partial E}{\partial t} + \frac{\partial}{\partial x_i}\left[u_i(\mathrm{E}+\mathrm{p})\right] = \frac{\partial}{\partial x_i}\left(K\frac{\partial T}{\partial x_i}\right) + \frac{\partial}{x_i}\left[u_i(\tau_{ij})_{eff}\right] \tag{5}$$

With

$$\mathrm{E} = \rho\left[c_v \mathrm{T} + \frac{1}{2}\left(u_{ii}{}^2\right) + \sum_{\mathrm{j=1,\,esp}} Y_j \mathrm{h^o}_j\right] \tag{5a}$$

$$\frac{\partial \rho \mathrm{k}}{\partial t} + \frac{\partial}{\partial x_i}(\rho \mathrm{ku}_i) = \frac{\partial}{\partial x_i}\left(\alpha_k \mu_{\mathrm{eff}}\frac{\partial k}{\partial x_i}\right) + \mathrm{G}_k - \rho\varepsilon \tag{6}$$

$$\frac{\partial \rho\varepsilon}{\partial t} + \frac{\partial}{\partial x_i}(\rho\varepsilon \mathrm{u}_i) = \frac{\partial}{\partial x_i}\left(\alpha_\varepsilon \mu_{\mathrm{eff}}\frac{\partial \varepsilon}{\partial x_i}\right) + \mathrm{C}_{1\varepsilon}\frac{\varepsilon}{k}G_k - C_{2\varepsilon}\,\rho\frac{\varepsilon^2}{k} - R_\varepsilon \tag{7}$$

$$\frac{\partial \rho Y_k}{\partial t} + \frac{\partial}{\partial x_i}(\rho Y_k u_i) = \frac{\partial}{\partial x_i}\left(D_{mk}\rho\frac{\partial Y_k}{\partial x_i}\right) + S_k \tag{8}$$

The equations for Eddy Dissipation Concept (Magnussen, 1977) consider that chemical reactions are determined by the rate of dissipation of the eddies, as follows:

$$R_{fu} = -C_R \rho Y_{fu}\frac{\varepsilon}{k} \tag{9a}$$

For local lean mixtures, oxygen will be the controlling of the reaction rate where St is the stoichiometric oxygen to burn.

$$R_{ox} = -C_R \rho \frac{Y_{ox}}{st}\frac{\varepsilon}{k} \tag{9b}$$

In the case of premixed flames, for local low products of combustion, the rate is.

$$R_{pr} = -C_R \rho \frac{Y_{pr}}{(1+st)}\frac{\varepsilon}{k} \tag{9c}$$

The Arrhenius kinetic rate is calculated as follows:

$$R_{fu,kinetic} = -A_{1\rho}^{-a} c_{fu}^{b} c_{ox}^{c} \exp\left(\frac{-E}{RT}\right) \tag{10}$$

Table 2. Details of the numerical model.

Case	Isothermal	Reactive Eddy Dissipation Concept (EDC)
CFD code	OpenFOAM	
Temporal formulation	Steady	Transient
Mesh	0.5, 2.1 and 5 million hexahedral cells	0.5, 2.1 and 5 million hexahedral cells
Pressure-Velocity coupling	SIMPLE	PIMPLE
Gradient scheme	Second-order (Gauss Linear)	
Divergence scheme	Second-order (Gauss Linear)	
Laplacian scheme	Second-order (Gauss Linear)	
Turbulence model	$k-\varepsilon$ standard	
Solver	simpleFoam	reactingFoam
Flow properties		
Density	1.225 [kg/m^3]	
Viscosity	1.7894.10-5 [kg/ms]	
Boundary conditions		
Axial inlet	Mean axial velocity: 0.52 [m/s] Turbulence intensity: 12% Turbulence kinetic energy: 0.00195 [m^2/s^2] Turbulence kinetic energy dissipation: 0.0344993 [m^2/s^3] -	Stoichiometric condition: CH_4: 5% Ar: 95% O_2: 0%
Annular inlet	Mean axial velocity: 1.66 [m/s] Mean tangential velocity: $v_\theta = S * v_z$ Turbulence intensity: 7.5% Turbulence kinetic energy: 0.015 [m^2/s^2] Turbulence kinetic energy dissipation: 0.0155 [m^2/s^3] -	Stoichiometric condition: CH_4: 0% N_2: 77% O_2: 23%
Outlet	Outlet static pressure: 101325 [Pa]	
Walls	Standard wall functions	

The local rate of combustion for EDC is the lowest reaction rate of equations 9 and 10, as follows:

$$R_{ch4} = -min\left[-R_{fu}; -R_{ox}; -R_{pr}; -R_{fu,kinetic}\right] \quad (11)$$

Incidentally, Eqs. (3), (4), (6) and (7) above are associated with the isothermal case.

The SIMPLE algorithm is used in this work to handle pressure–velocity coupling, due to its accuracy, reliability and stability in simulating swirling flows without reaction [16]. The z-axis is identified as the central axis of the chamber.

Table 2 summarizes the boundary conditions, flow properties and numerical details of the utilized model.

At the annular entrance, the expression for the free vortex is $\vec{V} = \left(\frac{-Dy}{x^2+y^2}, \frac{Dx}{x^2+y^2}, v_z\right)$,, where $D = \bar{r} * v_\theta = constant$.

One of the main uncertainties when modeling a swirl generator is the lack of specific details regarding the geometry of the airfoils. References (Wang, 2026; Yu, 2026 and Vivoli 2025) demonstrate the variety of swirl generators, from blades to plates or vanes. A common denominator is the desire to avoid secondary currents and pressure losses. Considering the abovementioned statements, the free vortex was chosen to conduct this study. Essentially, the decision to use the free vortex rests on the lack of geometrical details of the swirl generator in the test for the non-reactive case and the convenience of reducing the mesh elements in the annular nozzle to increase the spatial resolution of the combustion chamber. In this zone, the most relevant phenomena occur and, consequently, it becomes necessary to model it as best as possible. With the resulting mesh, the flame could be characterized effectively by applying reactive models.

4 Code validation and mesh independence

The mesh resolution was varied to study its effect on the accuracy of the results. Due to the complex flow patterns inside the chamber, one of the principal goals is to capture the main flow characteristics. Automatic meshing in OpenFOAM can be performed to obtain structured or unstructured meshes. Of these, structured meshes show better convergence performance and minimize diffusion errors (especially near solid boundaries) as they are characterized by a regularly repeated primitive shape in space, resulting in a regular topology. The use of flow-aligned hexahedral elements in structured meshes can improve the solution accuracy with a minimal number of cells; however, the mesh topology can be time-consuming to create. Pietroni (2023) provides a list of hex-mesh processing algorithms. A hexahedral mesh was adopted to avoid numerical diffusion errors, and because its use with OpenFOAM® significantly increases the number of convergence patterns with reference to tetrahedral meshes. Three different configurations with 0.5, 2.1 and 5 million cells were established.

To study the mesh independence, a systematic convergence assessment was conducted across three grid resolutions using the global error norms E_{L1}(MAE), E_{L2}(RMSE), and maximum error $E_{L\infty}$, together with their corresponding Grid Convergence Index (GCI) values. The procedure is detailed in (Celik *et al.*, 2008). These metrics quantify, respectively, the average, quadratic, and maximum pointwise discrepancies between two correlative meshes from the coarsest of 0.5 million cells to the finest of 5 million cells are summarized in table 3. The GCI provides a normalized measure of the uncertainty associated with discretization. The results indicate progressively stronger convergence for larger number of cells. The grid resolution shows a reasonable asymptotic regime.

To study the accuracy of the models, the numerical results and experimental data regarding the axial and tangential velocities in representative sections of the chamber were compared. Figure 2 depicts some of these results, which confirm reasonable agreement when using the mesh with 5 million cells.

Table 3. Comparative convergence for the three meshes.

Grid refinement factor	MAE	RMSE	L_∞	GCI
r_{21} = 1,7	0.135	0.165	0.301	16.9%
r_{32} = 1,59	0.043	0.056	0.083	5.4%

The results indicated higher errors for tangential velocities compared with axial velocities, where the mesh with 2.1 million cells yielded discretization errors of 18.2% and 9.5%, respectively, while those for 5 million cells were 11.5% and 7.5%, respectively. Overall, the discretization error obtained with the 5 million cell mesh was considered acceptable. The axial velocity errors indicated that the models were able to capture the longitudinal dimension of the IRZ in the central axis (which starts when the axial velocity turns from a positive to a negative value and finishes where it changes from a negative to a positive value).

The numerical results were in reasonable agreement with the flow patterns obtained experimentally by Roback and Johnson (1983) in all sections for all velocity components (i.e., axial, radial and tangential).

Burners with swirling flows have certain characteristic flow patterns; for example, the incoming flow expands in the radial direction and decelerates. If this deceleration is high enough, a recirculation zone is produced in the central axis (IRZ). On the other hand, an outlet recirculation zone (ORZ) is created in the corner between the expanding part and the walls of the chamber, even if the flow is not swirling. The interface between the recirculation zones has high shear and, consequently, promotes mixing. In figure 3 the green surfaces evidence the IRZ and ORZ. In Figure 4, the black curved lines represent iso-lines of zero axial velocity, characterizing the size, position and contour of the recirculation zones.

5 Mixing model

Next, the mixing level of the coaxial flows is analyzed. It is modeled at the macro- and meso-scales via turbulent convection and turbulent diffusion, using two different methods described by the following equations:

$$\frac{\partial}{\partial x_i}(\rho u_i Y) = \frac{\partial}{\partial x_i}\left(\rho D_t \frac{\partial Y}{\partial x_i}\right) \tag{12}$$

$$\frac{\partial}{\partial t}(\rho A) + \frac{\partial}{\partial x_i}(\rho u_i A) = \frac{\partial}{\partial x_i}\left(\rho D_t \frac{\partial A}{\partial x_i}\right) + \rho \tag{13}$$

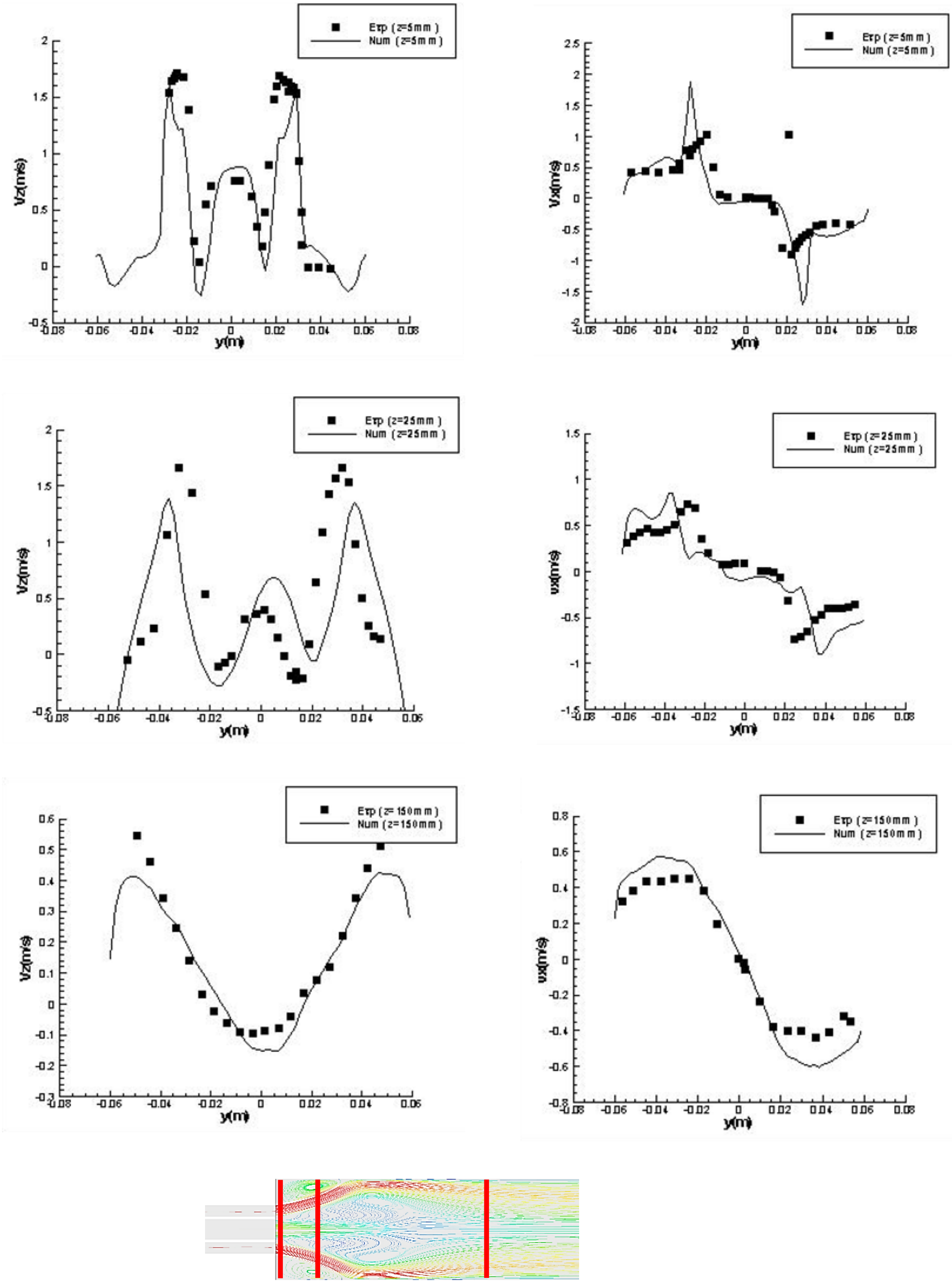

Figure 2. Radial distribution of axial velocity (left column) and tangential velocity (right column). Experimental results from Roback and Johnson for certain sections: upper line 5 [mm], middle z = 25 [mm] and lower line 150 [mm].

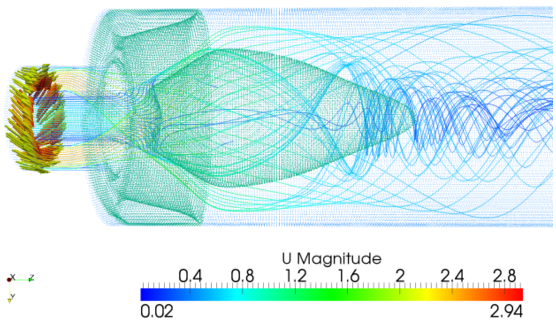

Figure 3. Diagram of vectors and velocity streamlines for the annular inlet with a free vortex, with iso-surface of zero axial velocity shown in green. Numerical results obtained with swirl number = 1, isothermal model, simpleFoam solver, k-ε standard turbulence model and 5 million cells.

where D_t is the turbulent diffusion coefficient. Equation (12) represents the transport equation for the passive scalar, Y, where the boundary condition corresponds to unity at the axial inlet and zero at the annular inlet. The computed field allows us to analyze mixing and the zones where it is favored. The upper half of Figure 4 depicts the fully developed field of the passive scalar, from which it can be seen that mixing is considerably favored due the recirculation zones. The incoming flow expands in the entrance of the chamber and then meets the flow in the IRZ; the most favorable condition is at the interface between the front of the axial inlet and the IRZ. After the flow has fully developed, the minimum value for the passive scalar is around 0.075. In the absence of values equal to 0 or 1, this means that all the incoming axial flow is mixed in different proportions with the incoming annular flow inside the chamber.

Meanwhile, Equation (13) describes the field for the age of the fluid, where A is the age of the fluid or the time of residence of the flow inside the chamber. The boundary condition corresponds to zero at both inlets, and because of the source term, it increases every timestep. The initial conditions were the converged flow filed for the steady state isothermal case. This equation is solved in transient form until achieving convergence.

The lower half of Figure 4 illustrates the age of fluid, representing the residence time of the flow when it enters the chamber until it leaves. The incoming flow is not mixed immediately with the IRZ; instead, it expands in the chamber, later becoming confined inside the IRZ for a certain period of time until finally returning to its ordinary upstream flow and reaching the exit. Quantitatively, the residence time in the IRZ is longer than that in the ORZ.

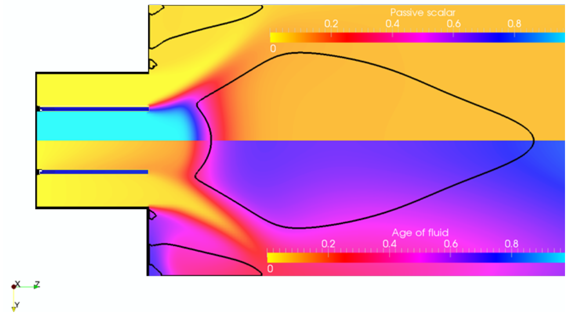

Figure 4. Upper half: Passive scalar field for S = 1. Lower half: Age of the fluid [s] for S = 1 in the range of 0 to 1 [s].

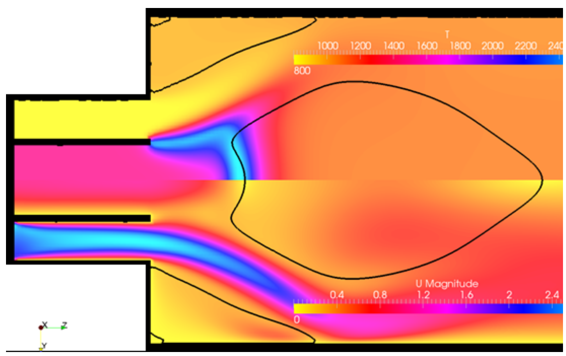

Figure 5. Temperature [K] (upper half) and velocity [m/s] (lower half) fields in the entrance of the chamber at S = 1.

6 Combustion modeling

An EDC-based combustion model was constructed to analyze the simplified chemical structure of the flame, as well as the velocity and temperature distributions in the chamber. In this way, it was possible to identify the position of the flame and quantify the heat released from the chemical reaction. Thereby, the best operating conditions (i.e., those that produce the highest heat release from the flow) were determined at given swirl numbers. To accomplish this, a mesh comprising 5 million cells was used.

Properties such as the specific heat capacity vary with the temperature and the local composition of the fluid.

In Figure 5, the velocity and temperature distributions are plotted for a swirl number equivalent to unity. Similarly to the passive scalar results, it can be observed that larger temperatures are reached in the region where the axial incoming flow meets the IRZ.

As the flame is diffusive, it locally behaves in either a rich or lean manner. Each point in the combustion chamber represents a local behavior. Being the burner thermally insulated, the heating of recirculating gases represents an internal redistribution

Table 4. Swirl number and their corresponding annular inlet velocities effect on maximum Damköhler value.

Swirl number	0.2	0.43	0.48	0.8	1	1.2	1.4
$v_\theta = f(r)$	0.00743/r	0.0159/r	0.0178/r	0.0297/r	0.0371/r	0.0446/r	0.052/r
Maximum local Damköhler number	0.6	1.3	1.55	1.58	1.55	1.75	

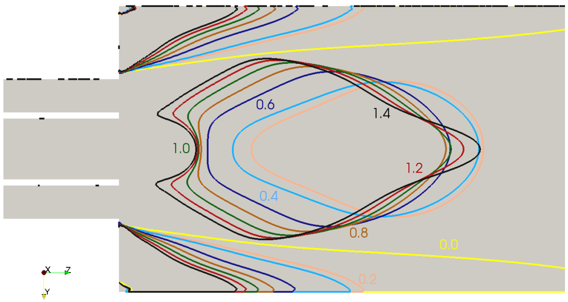

Figure 6. Iso-lines of zero axial velocity for different swirl numbers.

of energy, hence the local flame behavior is affected; for example, due to the heating of recirculating zones or heat gains from the combustion gases. Therefore, the local temperature in the reaction zone does not necessarily coincide with the adiabatic temperature corresponding to the mass fraction of methane present at each point; in particular, most points have temperatures below the adiabatic temperature.

7 Influence of the swirl number

The impact of varying swirl number values on the flow pattern was examined conjointly, with representative values listed in Table 4. Figure 6 outlines the iso-lines of axial velocity equal to zero for various swirl numbers, which serves to characterize and compare the size and geometry of the associated recirculation zones.

As the swirl number increases, the size of the IRZ increases, and vice versa. Moreover, at a swirl number equal to S = 0.45, the effects necessary for the creation of the IRZ were not observed. The flow expands in the chamber upstream of the ORZ. At S = 1, the ORZ is smaller and the incoming flow meets a larger IRZ.

To ascertain the swirl number values capable of enhancing the mixing effect, the Damköhler number was evaluated. There are different definitions depending on the importance of radiation, turbulence, ... In turbulent this work, the Damköhler number represents the ratio between the turbulence time scale t_t (residence time) and the chemical reaction time scale t_c. The definition of the Damköhler number is

$$Da = \frac{t_t}{t_c} \tag{14}$$

with the expanded form

$$Da = \frac{dQL}{\rho U c_p T} \tag{15}$$

where dQ is the heat flow, L is the characteristic length, ρ is the density, U is the velocity, c_p is the specific heat and T is the temperature.

Very small values of Da signify that the turbulence is faster than the chemical reaction; in this case, the flame is controlled by the reaction kinetics. In contrast, sufficiently large values of Da signify that the kinetics are effectively instantaneous and controlled by turbulent mixing. Within the scope of this study, the magnitude of the Da number is evaluated along the central axis, as the representative zone of combustion.

Damköhler numbers greater than unity were observed when the swirl number was equal to S = 0.43, 0.45, 0.8, 1, and 1.2. This was attributed to the ability of the swirl number to modify the size and position of not only the IRZ, but also the ORZ. Experimental work of reference (Kariuki et al, 2016) claims that methane-air flame extinction occurs at Da values close to unity, using a different definition based on the flame velocity of propagation. Igniting the jet at any given downstream location would lead to flame blowoff, with some studies having identified low Damköhler numbers as being related to flame blowoff (Cuoci *et al.*, 2013) In this study, lower Damköhler numbers are related to low swirl numbers and an IRZ located farther from the injector, thus increasing the risk of blowoff.

For swirl numbers greater than unity, the Damköhler number attained higher values.

Conclusions

The main conclusions that may be drawn from this work are based on a rigorous evaluation of the mixing quality for isothermal cases, achieved through numerical solution of the transport equations for the passive scalar and age of fluid values.

Through the implementation of a numerical model, it was possible to appraise the mixing quality at the macro-scale throughout the whole domain with respect to the passive scalar. This provides a useful tool that facilitates understanding of the balance between the mixing quality and variations in controllable parameters, such as the geometry, swirl number and inlet velocity. With regard to the age of the fluid, the residence time was also easily analyzed through the numerical approach. This turns out to be a relevant parameter with respect to the efficiency of combustion, leading to minimal NOx emissions under optimal conditions. In essence, this phenomenon arises as the reaction is directly related to the exposure time of the combustion products at high temperatures. A previous study has established that the flow field is governed by the flow rate and chamber geometry at high swirl numbers (Adam *et al*., 2025).

In addition, the flow pattern and main parameters—including the velocity field, position and size of the recirculation zones, temperature distribution, heat transfer and mixture composition—were easily established with the proposed model. It was possible to study the influence of the swirl number on the combustion quality through calculating the maximum Damköhler number along the central axis as the ratio between the turbulence time scale and the chemical reaction time scale, with the results demonstrating that Damköhler numbers greater than unity were obtained when the swirl number was higher than S = 0.43.

For this study, the open-source CFD codes in OpenFOAM® were employed. Additionally, the reliability of the results was found to be acceptable, due to their good agreement with previously reported experimental results and considering the complexity of the obtained flow pattern for swirling flows in confined chambers (e.g., recirculation zones, high gradients for velocity, pressure and temperature).

Acknowledgements

The authors acknowledge PRACE for awarding us access to resource Curie-GENCI@CEA based in France and MareNostrum@BSC based in Spain (Ref. 2010PA1766). We acknowledge that the results of this research were achieved using the DECI resource ARIS based in Greece at GRNET with support from the PRACE aisbl (Ref. SWIRLLES Tier-1, DECI-14). The seeds of the work were performed under the HPC-EUROPA2 project (project number: 228398) with the support of the European Commission - Capacities Area - Research Infrastructures.

Nomenclature

EDC	Eddy Dissipation Concept
IRZ	Inner Recirculation Zone
ORZ	Outer Recirculation Zone
RANS	Reynolds-Averaged Navier-Stokes
S	Swirl number

References

Adam A., Elbaz A., Kai R., Watanabe H. A Numerical Investigation of the Flame Characteristics of a CH4/NH3 Blend Under Different Swirl Intensity and Diffusion Models. *Energies* (**2025**), 18, 3921. https://doi.org/10.3390/en18153921

Bennett B. A. V, McEnally C. S, Pfefferle L. D., Smooke M. D., Computational and experimental study of axisymmetric coflow partially premixed methane/air flames, *Combustion and Flame*, Volume 123, Issue 4, (**2000**) 522-546 https://doi.org/10.1016/S0010-2180(00)00158-9

Celik I.B., Ghia U., Roache P.J., *et al*.,Procedure for Estimation and Reporting of Uncertainty Due to Discretization in CFD Applications. J. *Fluids Engineering*. 130(7) (**2008**), 078001 https://doi.org/10.1115/1.2960953

Cuoci A., Frassoldati A., Faravelli T., Ranzi E., A computational tool for the detailed kinetic modeling of laminar flames: Application to C_2H_4/CH_4 coflow flames, *Combustion and Flame* 160 (**2013**) 870–886 https://doi.org/10.1016/j.combustflame.2013.01.011

Iyogun C. O., Birouk M., Kozinski J. A., Experimental investigation of the effect of fuel nozzle geometry on the stability of a swirling non-premixed methane flame, *Fuel*, Volume 90, Issue 4, (**2011**) 1416-1423 DOI 10.1016/j.fuel.2010.12.033

Kariuki J., Dowlut A., Balachandran R. Mastorakos E. Heat Release Imaging in Turbulent Premixed Ethylene-Air Flames Near Blow-off. *Flow Turbulence Combust* (**2016**) 96:1039–1051 DOI https://doi.org/10.1007/s10494-016-9720-y

Kassem H. I., Saqr K. M., Aly H. S., Sies M. M., Wahid M. A., Implementation of the eddy dissipation model of turbulent non-premixed combustion in OpenFOAM, *International Communications in Heat and Mass Transfer* 38 (**2011**) 363–367 doi: https://doi.org/10.1016/j.icheatmasstransfer.2010.12.012

Lai Z., Wanga Q., Li J., Songa W., Suna B., Wanga S. Numerical investigation of hydrogen content effect on the combustion characteristics of blended hydrogen–methane bluff-body stabilized swirl flames. *International Journal of Heat and Fluid Flow* 117 (**2026**) 110078 https://doi.org/10.1016/j.ijheatfluidflow.2025.110078

Li B. W., Keeton B. W., Nomura K. K., Sánchez A. L., Williams F A.. A numerical investigation of H2-air lifted flames in swirling fuel injectors. *Combustion and Flame* 282 (**2025**) 114461 https://doi.org/10.1016/j.combustflame.2025.114461

Lin W., Zhang W., Liu H, Gao Z., Cai X., Wang J., Huang Z. Flame mode transitions in outer recirculation zone of lean premixed prevaporized n-decane/air swirling flames. *Experimental Thermal and Fluid Science* 168 (**2025**) 111502 doi https://doi.org/10.1016/j.expthermflusci.2025.111502

Magnussen B.F., Hjertager B.H., On mathematical modeling of turbulent combustion with special emphasis on soot formation and combustion, Symposium (International) on Combustion 16 (1) (1977) 719–729. https://doi.org/10.1016/S0082-0784(77)80366-4

Martínez-Gutiérrez, N., Ibarra-Bracamontes, L. A., Fuentes-Cortés, L. F., & Galván-González, S. R. (2026). Numerical modeling of synovial fluid behavior considering Newtonian and non-Newtonian approaches. *Revista Mexicana de Ingeniería Química*, 25(2). https://doi.org/10.24275/rmiq/Sim26649

Mesquita L. C. C., Vié A. and Ducruix S. On the interdependence between flame shape and vortex breakdown mode in turbulent swirling reacting flows. *J. Fluid Mechanichs* 1026 (**2026**) A34 https://doi.org/10.1017/jfm.2025.10937

Messig D., Hunger F., Keller J., Hasse C., Evaluation of radiation modeling approaches for non-premixed flamelets considering a laminar methane air flame, *Combustion and Flame* 160 (2013) 251–264 10.1016/j.combustflame.2012.10.009

Molina-Herrera, F. I., Montes-Rosales, H., Maldonado-Sierra, N. E., Sandoval-Hernández, M. A., Martínez-González, G. M., López-González, M. L., & Jiménez-Islas, H. (2026). Direct numerical simulation of the two-dimensional differentially heated square cavity at high Rayleigh numbers ($Ra \leq 10^{12}$). *Revista Mexicana de Ingeniería Química*, 25(2). https://doi.org/10.24275/rmiq/Fen26778

Pfeiler C., Raupenstrauch H., Application of Different Turbulence Models to Study the Effect of Local Anisotropy for a Non-Premixed Piloted Methane Flame, *Computer Aided Chemical Engineering*, Volume 28, (**2010**) 49-54 https://doi.org/10.1016/S1570-7946(10)28009-4

Olivani A., Solero G., Cozzi F., Coghe A., Near field flow structure of isothermal swirling flows and reacting non-premixed swirling flames, *Experimental Thermal and Fluid Science*, Volume 31, Issue 5, (**2007**) 427-436 https://doi.org/10.1016/J.EXPTHERMFLUSCI.2006.05.003

Pietroni N., Campen M., Sheffer A., Cherchi G., Bommes D., Gao X. Hex-Mesh Generation and Processing: A Survey. *ACM Transactions on Graphics*, 42/2 (**2023**) 16 https://doi.org/10.1145/3554920

Roback R., Johnson B.V. Mass and momentum turbulent transport experiments with confined swirling coaxial jets, *NASA CR-168252* (**1983**) https://ntrs.nasa.gov/api/citations/19840012473/downloads/19840012473.pdf

Syred N., Beer J.M., Combustion in swirling flows: A review, *Combustion and Flame*, Volume 23, Issue 2, (**1974**) 143-201 https://doi.org/10.1016/0010-2180(74)90057-1

Tlatelpa-Becerro, A., Castro, L., Rebolledo Abri, M., Avilés-López, I. S., Navarrete-Procopio, M., Zezatti-Flores, V. M., & Castañeda Magadán, E. O. (2026). Numerical-experimental study of a solar dryer using Computational Fluid Dynamics (CFD) for its optimization. *Revista Mexicana de Ingeniería Química*, 25(1). https://doi.org/10.24275/rmiq/Sim26720

Vignat G., Durox D., Candel S. The suitability of different swirl number definitions for describing swirl f lows: Accurate, common and (over-) simplified formulations. *Progress in Energy and Combustion Science* 89 (**2022**) 100969 https://doi.org/10.1016/j.pecs.2021.100969

Vivoli R. Goktepe B. Pugh D., Morris S., Bowen P. Valera-Medina A. Insights from swirl number and ambient pressure variations with a hydrogen/ammonia swirl stabilized diffusion flame. International Journal of Hydrogen Energy 190 (2025) 151941 https://doi.org/10.1016/j.ijhydene.2025.151941

Wang D., Khalatov A., Shi-Ju E., Borisov I , Stupak O., Donyk T. Flow structure and heat transfer in subsonic nozzle with initial flow swirl *International Journal of Thermal Sciences* 224 (**2026**) 110712 https://doi.org/10.1016/j.ijthermalsci.2026.110712

Xu H., Pang L., Zhao N., Zheng H. Effects of fuel staging strategy on combustion and emissions in a centrally-staged swirling combustor: experimental and numerical investigations. *Fuel* 406 (**2026**) 136961 doi 10.1016/j.fuel.2025.136961

Yu B., Li M., Li S., Zhang J., Zhao Y.. Effect of swirl blade angles on the combustion and emission characteristics of a novel cavity-swirler-based combustor. *Applied Thermal Engineering* 279 (**2025**) 128077 DOI 10.1016/j.applthermaleng.2025.128077

Yu H., Yang S., Wang H. CFD-enhanced co-design framework of industrial-scale multi-scale coaxial swirling lance Chemical Engineering Science 326 (2026) 123543. Doi https://doi.org/10.1016/j.ces.2026.123543

Zhen H. S., Leung C.W., Cheung C.S., A comparison of the thermal, emission and heat transfer characteristics of swirl-stabilized premixed and inverse diffusion flames, *Energy Conversion and Management*, Volume 52, Issue 2, (**2011**) 1263-1271 https://doi.org/10.1016/j.enconman.2010.09.023